Iron and manganese oxides from the oxidation zone of the Ľubietová-Podlipa deposit

Juraj Majzlan[1], Martin Števko[2], Martin Chovan[3], Stanislava Milovská[2], Stanislav Jeleň[2], Tomáš Mikuš[2] & Adrián Biroň[2]

[1] Institut für Geowissenschaften, Friedrich-Schiller-Universität, Burgweg 11, 07749 Jena, Germany
[2] Ústav Vied o Zemi Slovenskej Akadémie Vied, Dúbravská 9, 840 05 Bratislava, alebo Ďumbierska 1, Banská Bystrica, Slovakia
[3] Katedra mineralógie, petrológie a nerastných surovín, Univerzita Komenského, Ilkovičova 6, SK-842 15 Bratislava, Slovakia

AGEOS

Abstract: Ľubietová-Podlipa is a small historical Cu deposit in the Veporic unit of the Central Western Carpathians in Slovakia. It is the type locality of libethenite and mrázekite. The oxidation zone of the deposit contains copious pseudomalachite and malachite that attracted the attention of mineralogists and mineral collectors for a long time. Another abundant group of supergene minerals, Fe and Mn oxides and oxyhydroxides (collectively called oxides here), received much less attention and were investigated closely in this work. Bulk analyses of the oxidation zone (channel samples) showed that it is rich in Cu (average 7070 ppm), Mn (430), Zn (650), Ba (640), Bi (235). Concentrations of other elements are low, such as Co (49), Ni (47), Sb (47), W (96), or Ag (1.2). Some of the elements are concentrated by Mn oxides. The Fe and Mn oxides formed mostly by weathering of chalcopyrite and Fe-dolomite. They coat the Cu minerals but may also be the substrate for the growth of the Cu minerals. The Mn oxides are flaky, with individual particles less than 5 μm large and less than 1 μm thick. The particles accumulate in spherical aggregates with size of tens of micrometers. Raman spectroscopy and powder X-ray diffraction indicate that the Mn oxides are most likely mixtures of birnessite and asbolane, with minor amount of tectomanganates (e.g., hollandite). They accumulate CuO (average of electron microprobe analyses 21.8 wt.%), CoO (5.5), BaO (1.0), CaO (0.5), and K_2O (0.5) in their structure. Fe oxides occur either as brick-red, massive pseudomorphs after chalcopyrite or as coatings and crusts on fractures. They were identified as hematite or goethite, commonly intergrown. Hematite crystals may be embedded in pseudomalachite and Fe and Mn oxides intergrown in tufts. Fe oxides adsorbed As, Sb, and Bi, when available, but the concentrations of these elements are usually low (< 1.5 wt.%). Fe oxides may be rich in P_2O_5 (average 2.78 wt.%), SiO_2 (1.67), Al_2O_3 (0.22), and CuO (6.47). Locally elevated Bi concentrations led to precipitation of rare bismutite. Because of their abundance and retention capacity for certain elements, Fe and Mn oxides influenced the composition of the oxidation zone and the environmental mobility of the elements to a great extent.

Key words: Ľubietová; iron oxides; manganese oxides; supergene minerals

1. INTRODUCTION

The deposit Podlipa near the village of Ľubietová is located about 20 km E from the city of Banská Bystrica in central Slovakia. The host rocks belong to the Veporic unit of the Central Western Carpathians, represented by Permian siliciclastic rocks. In a wider region of the deposit, these rocks are associated with various types of paragneisses, orthogneisses, and amphibolites. These basement rocks underwent Variscan and Alpine metamorphism and are arranged in belts with a general NE-SW strike (Slavkay et al. 2004). The primary ore mineralization is epigenetic, made of quartz veins with Fe-dolomite, chalcopyrite, less common tennantite, and additional accessory minerals (Luptáková et al. 2016). The available data indicate that the deposit is genetically linked to the Alpine metamorphism in this region.

The deposit Podlipa is known for its well-developed oxidation zone and it is the type locality of libethenite ($Cu_2(PO_4)OH$, Breithaupt 1823) and mrázekite ($Bi_2Cu_3(PO_4)_2O_2(OH)_2 \cdot H_2O$, Řídkošil et al. 1992). Apart from these minerals, the oxidation zone is a host of rich accumulations of pseudomalachite and malachite. Less common supergene minerals include acanthite, azurite, bismutite, brochantite, camerolaite, chalcocite, chalcoalumite, corkite, cornwallite, covellite, cuprite, cyanotrichite, goethite, gypsum, kintoreite, langite, ludjibaite, native copper, olivenite, petitjeanite, pharmacosiderite, reichenbachite, and tenorite (Láznička 1965; Figuschová 1977; Hyršl 1991; Řídkošil et al. 1992; Luptáková et al. 2012; Milovská et al. 2014a; Števko et al. 2016, 2017, 2021; Majzlan et al. 2018; Števko, unpublished data). Despite intensive mineralogical research over centuries (from the 19th to the 21st century), one group of abundant supergene minerals received hardly any attention. These are ubiquitous iron and manganese oxides and oxyhydroxides (collectively called oxides here), associated with other supergene minerals or occurring separately in the oxidation zone and in the surrounding rocks. In this contribution, we aim to fill this gap and specifically address the chemical composition and nature of the Fe and Mn oxides. This work is a continuation of the modern mineralogical research by Števko et al. (2016, 2017, 2021) and Majzlan et al. (2018). Certain data on Mn oxides were already presented by Milovská et al. (2014a), the Fe oxides were not closely investigated yet.

2. MATERIALS AND METHODS

Samples for this work were collected in the underground spaces of the adits Horný Ladislav, Dolný Ladislav, and Reiner in the ore

Manuscript received 2025-05-31
Revised version accepted 2025-07-15

field Reiner (48.74748 °N, 19.38497 °E) or from the old dumps in the ore field Podlipa. Both of these ore fields constitute the deposit Podlipa. Many of these samples were also used in our recent work (Majzlan et al. 2025) for isotopic research of the supergene minerals and the elucidation of the formation of the oxidation zone.

The precise localization of the samples collected underground is shown in Fig. 1. Most of them (L-1 through L-46) were grab samples, but we also collected two channel samples (L-51 and L-52). Samples taken from the dumps were not precisely localized because their relation to the ore bodies cannot be established anyway.

Underground surveying of the Reiner mine was done using a Leica DistoX1 laser distance meter, 3-axis compass, and clinometer combined with PDA (Nautiz X8) equipped with PocketTopo application software. Horizontal and lateral projections of the mine with marked sampling locations are shown in Fig. 1.

The channel samples L-51 and L-52 were crushed, sieved, and homogenized. A representative sample for the chemical analyses was extracted by coning and quartering. It was completely digested in a mixture of HF, HNO_3, and $HClO_4$ in sealed Teflon vessels at 200 °C. The resulting solution was analyzed by ICP-MS for major, minor, and trace elements. The analyses were carried out with an X-Series II, ThermoFischer Scientific ICP-MS instrument. Silicon was not analyzed because of the known volatilization of Si during the digestion, which leads inevitably to systematic errors. The Si content was determined by X-ray fluorescence analysis in the work of Majzlan et al. (2025).

For quantitative whole-rock analyses, X-ray fluorescence (XRF) spectrometry was used, coupled with wavelength-dispersive detection of the emitted radiation. The XRF pellets were made of 4 g of the powdered rock sample and 1 g wax. The powder was thoroughly mixed by shaking for 15 min, pressed in a PW E30 hydraulic press with 294.2 kN, and analyzed under vacuum in a Philips PW 2404 wavelength-dispersive X-ray fluorescence spectrometer, equipped with a 4 kW Rh anode tube.

To obtain semiquantitative information on the elemental distribution in the studied samples, energy-dispersive micro-X-ray fluorescence spectrometry (μ-XRF) was performed using an M4 TORNADO spectrometer (Bruker). Elemental maps were acquired from a selected area within a polished rock containing veins of sulfide minerals. The excitation source, a rhodium anode, operated at 50 kV with a current of 600 μA. Measurements were conducted under vacuum of 20 mbar, with a spatial resolution of 20 μm between measurement points and a scanning speed of 20 ms per pixel. The fluorescence signal was collected by a silicon drift detector with a 30 mm^2 active area and a spectral resolution of 145 eV.

The grab samples were inspected visually for the presence of supergene minerals of interest, primarily for Fe and Mn oxides. If such minerals were present, parts of the samples were separated under a binocular microscope and finely ground in an agate mortar. The powder was analyzed by powder X-ray diffraction (pXRD) with the Bruker D8 Advance instrument using Si low background sample holders for small samples with or without a sample cavity. This instrument uses Cu Kα X-ray radiation generated at 40 kV and 40 mA and a Sol-XE silicon drift detector. The measurement step was 0.02° 2θ, and counting time of 1.25 s.

All grab samples were sawn, ground, and polished to prepare thin or polished sections for a detailed investigation in transmitted or reflected polarized light. Selected sections were coated with carbon, and the chemical composition of the minerals was

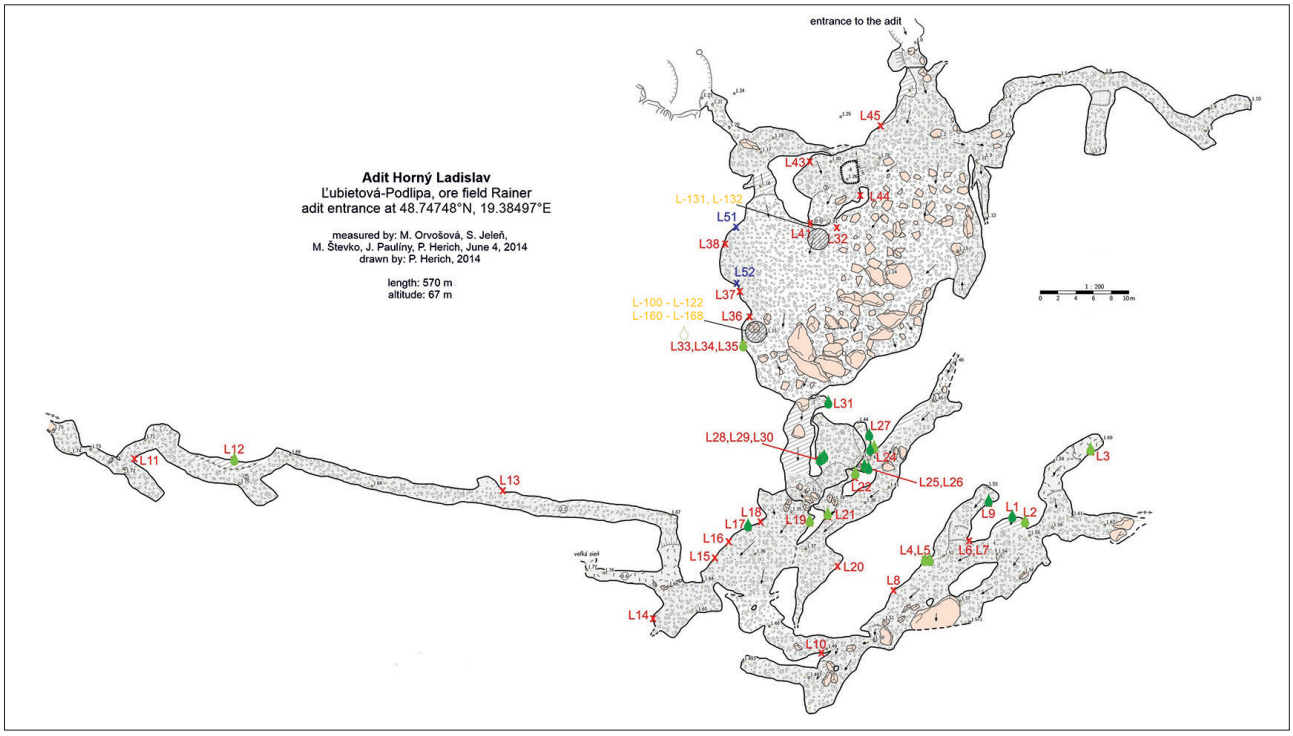

Fig. 1. Map of the sampled underground space with localization of the samples. Different color codes correspond to the sampling campaigns in different years. The channel samples are labeled blue.

investigated by electron microprobe analysis (EMPA) using a JEOL JXA-8230 at the University of Jena. The measurement conditions of wavelength-dispersive X-ray (WDX) analyses were set to an accelerating voltage of 15 kV, a beam current of 15 nA, and a beam diameter of 1- 5 μm. WDX was used to measure the following X-ray lines and elements: Kα of Na, Al, Mg, K, S, Ca, P, Mn, Fe, Cu, and Co; Lα of As, Ag, Sb, and Ba; as well as Mα of Pb and Bi. The standards used for calibration were albite for Na, corundum for Al, InAs for As, wollastonite for Si and Ca, periclase for Mg, orthoclase for K, barite for Ba and S, Ag_2Te for Ag, InSb for Sb, apatite for P, galena for Pb, pure metal standards (100 %) for Bi and Co, rhodonite for Mn, hematite for Fe, and cuprite for Cu. Counting times were set to 40 s to improve count-rate statistics. Overlap corrections were applied to avoid interference between the elements and lines of As and Bi, S and Co, Sb and K, Al and Ag ($Lα_1$ and $Lα_2$), Al and Ba, S and Co, Ba and Bi, P and Ca, Ba, and Cu, as well as Na and Pb. The detection limits were calculated from the background counts, the measurement time, and the standard material concentration, amount to 0.02 wt.% for Al, As, Si, Mg, S, P, Mn, Fe and Co; 0.03 wt.% for Ag and Cu; 0.04 wt.% for Bi, as well as 0.05 wt.% for Sb and Pb.

Unpolarized Raman spectra were measured using a Horiba Jobin-Yvon LabRam HR800 microspectrometer, mounted on an Olympus BX41 microscope, with a confocally coupled Czerny-Turner type monochromator (focal length 800 mm). A frequency-doubled Nd-YAG laser at 532 nm (Laser Quantum, UK) was used for excitation with power on the sample less than 24 mW (a series of tests at various power settings was performed due to possible thermal effects). The Raman-scattered light was collected in 180° geometry through a 50× objective lens and dispersed by a diffraction grating with 600 g/mm onto a cooled (–70 °C) charge-coupled device (CCD) detector. The grating turret accuracy was calibrated between the zero-order line and the laser line at 0 cm^{-1}. Spectral accuracy was verified on the 734 cm^{-1} band of Teflon, the system resolution was 6 cm^{-1}, and band definition was improved using a 2-fold sub-pixel shift. For each Raman spectrum, the baseline was subtracted (Labspec® v.5 software).

3. RESULTS AND DISCUSSION

3.1. Bulk chemical composition of the oxidation zone

The bulk chemical composition of the oxidation zone was documented by sparse historical data (Koděra et al. 1990) related to the richest parts of the ore body. These parts were mined out and are no longer available for sampling. In order to determine the chemical composition of the oxidation zone, we collected two channel samples and analyzed their material. In our previous work (Majzlan et al. 2025), we presented the analytical results from X-ray fluorescence (XRF) analysis. In this work, we focused on the major components of the oxidation zone, including SiO_2, and the XRF method was capable of analyzing this and other oxide components. The ICP-MS analysis, used here, is not able to give the correct concentration of SiO_2 (see above) but can provide information about many minor and trace elements. The results are listed in Table 1. In the following text, we list the average value of the analyses. We also point out that there are differences among the analytical techniques (XRF *versus* ICP-MS), and the estimated relative uncertainty of the ICP-MS data is about 5 %.

The channel samples captured both the mineralized zone and the host rocks represented by Permian meta-arcoses. In terms of major elements, the analytical data for the channel samples are reminiscent of the bulk composition of the meta-arcoses. The Cu content is, as expected, high, around 7070 ppm. The principal reservoirs of Cu in our samples are the minerals malachite and pseudomalachite, to a lesser extent, also libethenite. For comparison, the Mn content is 430 ppm. The Mn oxides, even though they are ubiquitous, are much less voluminous than the Cu supergene minerals. The Fe_2O_3 content is high, up to 3.2 wt.%. We note, however, that this value includes not only the supergene Fe oxides but also the rock-forming minerals, especially the common chlorites. The Ca concentration is low, only 49 ppm, documenting either low primary abundance of carbonates or their dissolution and aqueous transport during weathering.

Among elements that commonly enter the structure of Mn oxides, the most abundant one is Zn (650 ppm), followed by Ba (640 ppm), Co (49 ppm), and Ni (47 ppm). When compared to the bulk MnO concentration (430 ppm), however, it is clear that Mn oxides are not the only reservoir of these elements. The most abundant metalloid is Bi (235 ppm), which is sourced from the primary kupčíkite (Luptáková et al. 2016) or the supergene bismuth minerals (Števko et al. 2017). Arsenic is less abundant (119 ppm) but still exceeds the concentration of Sb (47 ppm) in the Mn oxides. The predominance of As over Sb complies with the prevalence of As over Sb in tennantite at the studied site (Luptáková et al. 2016). The Sn concentration is very low (9 ppm) even though the primary ores locally contain rare cassiterite (Luptáková et al. 2016). The concentration of W is higher (96 ppm), but no primary W minerals are known. The concentration of Ag is only 1.2 ppm, and that of Cd is 0.06 ppm.

3.2. Textures of supergene minerals in the oxidation zone

The primary ore body is essentially a silicified zone with low-grade chalcopyrite ore, hosted by quartz and carbonate (dolomite) gangue. Other sulfides are rare (Luptáková et al. 2016) but can be locally discerned by the presence of their oxidation products. The most common supergene minerals are pseudomalachite, libethenite, malachite, and Fe and Mn oxides. In the deeper parts of the mine, cuprite or rare native copper could be found, overgrown and corroded by malachite and pseudomalachite (Fig. 2).

Supergene copper minerals occur mostly in cavities and fractures. Libethenite commonly forms isometric crystals, lining the cavities in quartz. These cavities were not present in the primary ores. Their shape indicates that they are hollow spaces after dolomite crystals, in agreement with the earlier interpretation of Luptáková et al. (2016). In the deeper parts of the mine, unweathered dolomite and chalcopyrite may be found (Fig. 3), showing that sulfides penetrate into dolomite along its cleavage planes. Weathering of chalcopyrite released Cu, S, and generated sufficient acidity to dissolve carbonates. Within the oxidation

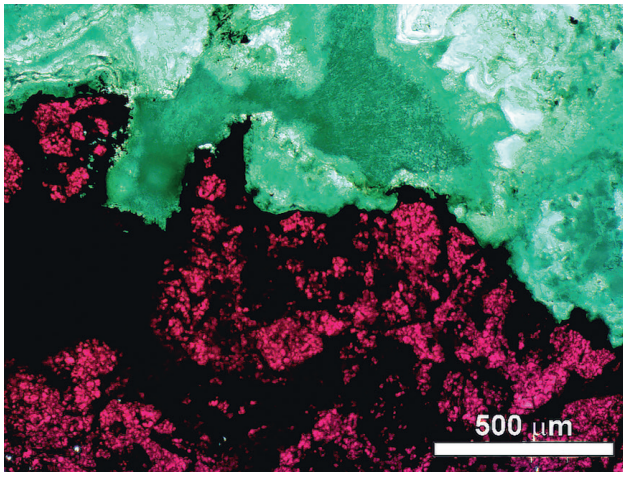

Fig. 2. Cuprite overgrown by a banded aggregate of pseudomalachite. Sample L-21, transmitted light, crossed nicols.

zone, primary carbonate minerals (mostly represented by Fe-dolomite) no longer exist. Pseudomalachite forms botryoidal aggregates with distinct growth zoning, made of many small platy crystals (Fig. 4a,b).

Iron and manganese oxides may form crude pseudomorphs after the primary chalcopyrite-dolomite aggregates. In this case, boxwork textures of the oxides are typical. Very often, the oxides coat fractures within the oxidation zone, attesting to the mobility of Fe and Mn prior to their oxidation. The Fe and Mn oxides occur also outside of the primary ore body. The Cu phosphates are mostly restricted to the primary zone, but they are often associated with Fe or Mn oxides.

3.3. Manganese oxides

Manganese oxides occur as black crusts, coatings, small circular aggregates, and void filling in quartz or in the fractures of the host rocks. They are found together with the supergene Cu minerals, particularly with pseudomalachite (Fig. 4a,b). They may cover pseudomalachite or libethenite, but, occasionally, they can be overgrown by aggregates of pseudomalachite. They do not form, however, dendritic aggregates that are very typical for this group of minerals. Guilbert and Park (2007, page 821) proposed that the circular aggregates (which they call "*spotty dendrites*") represent the typical morphology of Mn oxides formed in the presence of Cu in the aqueous solutions. According to them, the spotty dendrites are an excellent exploration criterion to detect oxidized portions of Cu deposits in the field. A detailed investigation of back-scattered electron images showed that the black crusts can be made of alternating layers of Mn and Fe oxides. The Mn oxides impose the black color and make the Fe oxides in such overgrowths difficult to spot.

Secondary-electron images of the Mn oxides (Fig. 4c,d) reveal their flaky morphology. The individual particles are less than 5 µm large and their thickness does not exceed 1 µm (Fig. 4d). The particles accumulate in spherical aggregates with a size of tens of micrometers. These aggregates combine into macroscopic crusts and spherules on quartz, host rocks, or supergene Cu minerals.

Identification of the mineral species among the Mn oxides is a demanding task. Powder X-ray diffraction datasets and Raman spectra point to the phyllomanganate nature of the studied Mn oxides. This group includes several minerals. Some of them place divalent or monovalent cations (e.g., Ca, Na) in the space between the layers, some incorporate such cations (e.g., Co, Ni) into the layers with octahedrally coordinated cations (Manceau et al. 1987, Post 1999).

Powder X-ray diffraction indicates that the studied manganese oxides could belong to birnessite, which prefers Na or Ca in its structure. Raman spectra are nearer to the mineral of asbolane, which prefers Ni or Co (Fig. 5). Raman spectra show bands in the range of 650-690 cm^{-1}, although the literature reported such bands in phyllomanganates (e.g., chalcophanite or ranceite) at max. 670 cm^{-1}. Tectomanganates (manganates with framework structures) have Raman bands at higher wavenumbers, around 740-760 cm^{-1}. Some powder X-ray diffraction datasets can be assigned to chalcophanite or cryptomelane, but Raman spectra from the same samples indicate birnessite or asbolane. Only a few Raman spectra can be interpreted in terms of the mineral

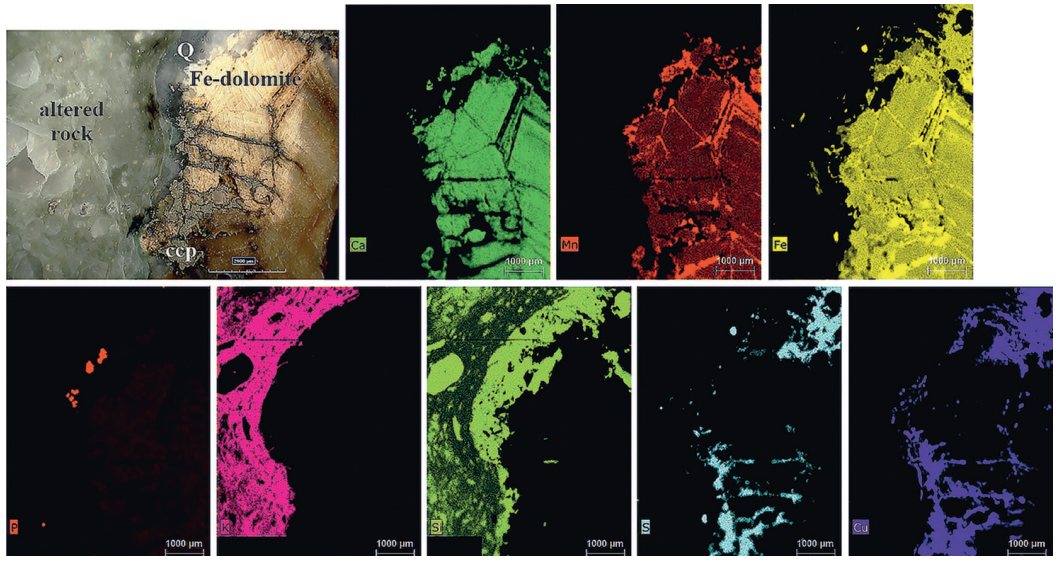

Fig. 3. Element distribution maps from an aggregate of primary Fe-dolomite, with accompanying veinlet of hydrothermal quartz (Q). Younger chalcopyrite (ccp) penetrates into the Fe-dolomite. The hydrothermal minerals are hosted by altered host rock with abundant illite and a few phosphate grains. Data acquired with the µ-XRF spectrometer.

hollandite. The interpretation of the data (both Raman and powder X-ray diffraction) is complicated by the poor crystallinity of the Mn oxides, broadening of the features (Raman bands, XRD peaks), and overlap of the features. The data indicate that the studied samples consist of mixtures of Mn oxides, dominated by birnessite or asbolane. Tectomanganates (hollandite) are much less abundant. The elevated Cu concentration (see below) could indicate that some of the analyzed material could belong to crednerite or cuproasbolane. Alternatively, the Mn oxides could contain nanoparticles of Cu minerals, such as native copper (e.g., Majzlan et al. 2018).

In terms of chemical composition, the Mn oxides are highly variable. The low analytical sums are undoubtedly caused by the presence of H_2O and porosity of the analyzed minerals. Representative analyses are listed in Table 2, all available analyses can be found in the electronic supplementary information.

The tendency of the Mn oxide to incorporate Co, Ba, and K into their structures is visible in the element distribution maps in Fig. 6. The Cu concentration is obscured by the surrounding pseudomalachite.

Apart from the major Mn, the Mn oxides take up Cu (average of electron microprobe analyses 21.8 wt.% CuO), CoO (5.5 wt.%), and BaO (1.0 wt.%) in their structure (Fig. 7a, c). In some of the analyzed compositions, CuO dominates over MnO_2 (Fig. 7d), and such oxides could be described as Mn-Cu oxides. Zinc is below the detection limit. On the other hand, calcium whose total concentration in the oxidation zone is much lower than that of Zn, enters the structures of Mn oxides (average 0.5 wt.% CaO). Another element that is accumulated by the Mn oxides is potassium (average 0.5 wt.% K_2O). Elevated concentrations of SiO_2 (2.8 wt.%) and P_2O_5 (0.4 wt.%) are most likely caused by adsorption of the tetrahedral units onto the surfaces of the Mn oxide particles.

3.4. Iron oxides

Iron oxides are present throughout the oxidation zone. There are two different modes of their occurrence. The first one is represented by massive, compact aggregates of several centimeters in size, the second one by omnipresent ochreous coatings in the ore bodies and in the host rocks.

The massive aggregates have brick-red color and are located only within the ore body. In the upper parts of the mine, they consist predominantly of Fe oxides, sometimes with small amount of Cu supergene minerals such as malachite. In the deeper parts, they may contain chalcopyrite relics in their core. These aggregates are therefore the product of chalcopyrite weathering. During this process, Cu and S are mobilized and re-distributed whereas Fe remains mostly *in situ*. During weathering, Fe is rapidly immobilized by oxidation to Fe(III) that is catalyzed in the presence of Cu species in the aqueous solution (González et al. 2016).

Mobility of Fe inside the oxidation zone is documented by hematite crystals embedded in pseudomalachite (Fig. 8a,b) and by banded overgrowths of Fe oxides with variable composition (Fig. 8e,f). They likely correspond to slow oxidation of Fe(II) transported in the aqueous solution. Some globular aggregates

Table 1. Chemical composition of channel samples from Ľubietová. The table compares the results of X-ray fluorescence analyses and analyses with ICP-MS after total digestion.

sample (method)	L-51 (ICP)	L-51 (XRF)	L-52 (ICP)	L-52 (XRF)
SiO_2 wt. %		83.10		88.18
TiO_2	0.28	0.27	0.27	0.25
Al_2O_3	6.22	7.70	4.99	5.67
Fe_2O_3	3.88	4.10	2.35	2.47
MnO	0.07	0.08	0.01	0.01
MgO	0.34	0.53	0.23	0.19
CaO	0.01	< DL	-	< DL
Na_2O	0.06	0.22	0.06	0.25
K_2O	2.06	2.75	1.57	2.00
P_2O_5	0.35	0.28	0.15	0.13
SO_3		< DL		< DL
LOI		1.70		1.39
Ag mg/kg	0.94		1.51	
As	142		95	
Ba	612	840	480	628
Bi	< DL		235	
Ca	66		31.4	
Cd	0.054		0.059	
Cl		109		100
Co	68	59	33	33
Cr	8.2	24	6.1	20
Cu	6190	7679	5986	8426
Li	8		6.1	
Mo	1.7		0.24	
Nb		8		7
Ni	47.6	69	27.7	43
Pb	11.493		19.11	
Sb	39.4		54.9	
Sn	11.5		5.98	
Sr	11.463	28	13.1	39
V	33	42	27.7	38
W	92		99	
Zn	25	1231	11.38	1333
Zr	62.5	110	51.4	106
Sc	5.947		4.594	
Rb	72.9	< DL	58.9	< DL
Y	12.9	18	13.6	18
Cs	3.65		2.99	
La	16.9		18.3	
Ce	35.95		38.3	
Pr	4.52		4.8	
Nd	19.1		20	
Sm	4.9		4.36	
Eu	1.298		1.07	
Tb	0.47		0.48	
Gd	3.4		3.07	
Dy	2.631		2.77	
Ho	0.496		0.504	
Er	1.37		1.41	
Tm	0.201		0.192	
Yb	1.22		1.18	
Lu	0.196		0.187	
Th	4.96		4.34	
U	1.99	< DL	2.303	< DL

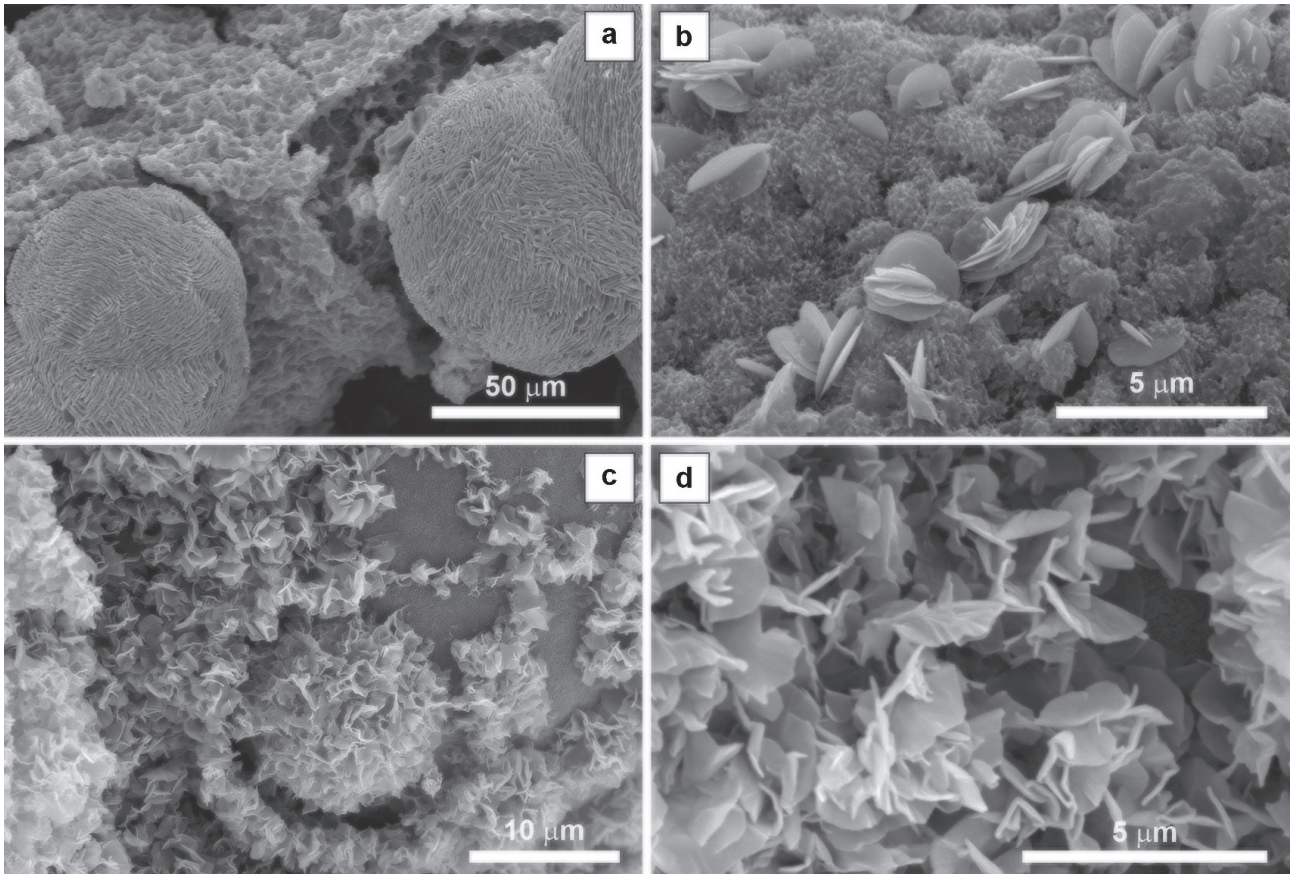

Fig. 4. Secondary-electron images of Mn oxides and associated minerals from Ľubietová. a,b) Polycrystalline aggregates of pseudomalachite grow on a crust of Mn oxides (a – sample L-125, b – sample L-101). c,d) Details of flaky morphology of the Mn oxides (sample LB-17-11).

of Fe oxides are overgrown by fine acicular crystals of Mn oxides, in agreement with the thermodynamic predictions that Fe(II) should be oxidized to Fe(III) before Mn(II) is oxidized to Mn(IV) (Fig. 8c). When viewed in a scanning electron microscope, such aggregates appear as tufts and whiskers of many tiny Fe oxide crystals, some of them covered by Mn oxides (Fig. 8d).

Table 2. Representative electron microprobe analyses of Mn oxides from Ľubietová-Podlipa. – = below detection limit. All data in weight %.

Sample	L–22B	L–22B	L–22B	L–22B	L–22B	L–24	L–33	L–132	L–132
Point	19	18	5	3	7	23	72A	6	1
Al_2O_3	0.54	0.47	0.58	0.65	0.65	0.3	0.05	0.56	0.33
As_2O_5	–	–	0.12	0.03	0.07	0.03	0.03	–	0.09
SiO_2	13.26	11.82	8.28	8.44	7.7	0.14	0.2	0.4	0.48
MgO	0.06	0.14	0.11	0.11	0.14	0.12	0.25	–	0.05
K_2O	–	–	–	–	–	–	0.25	1.46	1.46
SO_3	0.13	0.12	0.21	0.39	0.15	0.08	0.2	0.19	0.21
CaO	0.29	0.33	1.41	1.29	1.47	0.59	0.5	0.16	0.17
Ag_2O	0.03	–	0.03	0.03	0.03	–	0.04	–	–
Sb_2O_5	–	–	0.06	–	–	–	0.25	0.15	0.17
P_2O_5	0.3	0.29	0.3	0.25	0.25	0.18	0.22	0.67	0.72
PbO	–	0.06	0.09	–	0.04	0.03	0.42	–	–
Bi_2O_3	–	–	0.03	–	–	–	0.53	–	–
BaO	0.08	0.12	0.15	0.12	0.13	0.09	3.05	1.45	1.54
MnO_2	24.29	24.96	30.86	31.02	38.78	42.53	42.53	47.44	48.31
Fe_2O_3	3.83	3.40	1.20	1.21	0.77	4.98	2.28	1.54	4.80
CuO	32.14	30.82	33.68	32.72	35.36	22.14	12.32	11.62	10.51
CoO	4.64	4.3	2.62	2.66	2.75	11.73	7.08	2.4	2.15
ZnO	–	–	–	–	–	–	–	–	–
Total	**79.59**	**76.84**	**79.73**	**78.92**	**88.28**	**82.94**	**70.19**	**68.05**	**70.99**

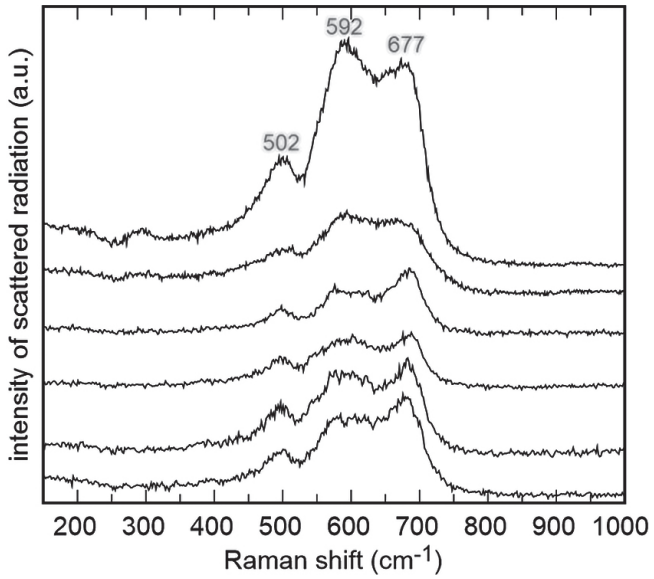

Fig. 5. Raman spectra of Mn oxides from Ľubietová. Positions of the most prominent bands were marked with the numerical value of their Raman shift.

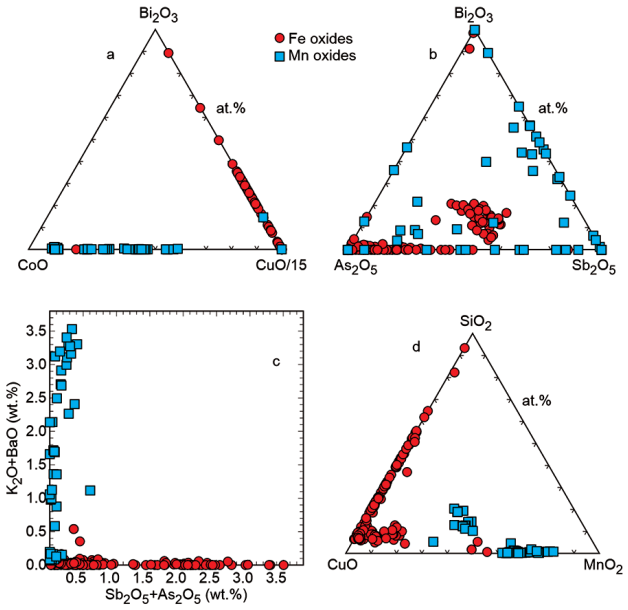

Fig. 7. Comparison of chemical composition of Fe oxides and Mn oxides on selected oxide components. All data from electron microprobe analyses.

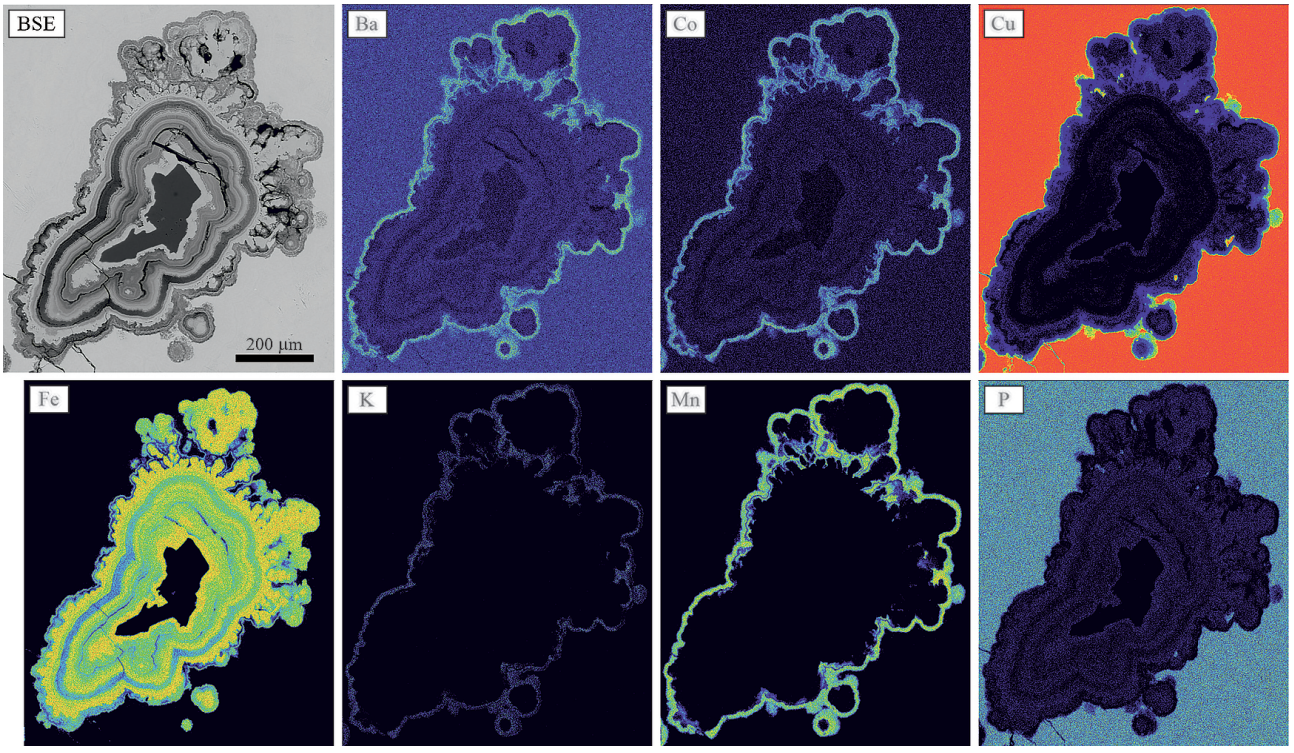

Fig. 6. Element distribution maps, sample L-132. Small aggregate of Fe oxides and Mn oxides is enclosed in pseudomalachite. Note the correlation of Mn in the Mn oxides with Ba, Co, and K. Data acquired by an electron microprobe.

Raman spectra of these Fe oxides show that they are a mixture of hematite and goethite (Fig. 9). The band assignment relies on the reference spectra (Lafuente et al. 2015) but also detailed work on Raman spectroscopy on Fe oxides (Hanesch 2009, Abrashev et al. 2020). Hematite is compact and may be overgrown by botryoidal layers of goethite or of alternating goethite and hematite. Iron oxides adsorb As, even though the oxidation zone at Podlipa contains not much of this element. Most of the Fe oxides have slightly elevated As concentration but little Sb or Bi (average As_2O_5 0.40 wt.% in this group) (Fig. 7, Tables 3 and 4). There is another, distinct group of Fe oxides that contain As, Sb, and Bi (0.85 wt.% As_2O_5, 1.30 wt.% Sb_2O_5, 0.51 wt.% Bi_2O_3 on average) (Fig. 7). We assume that Fe oxides with elevated As, Sb, and Bi formed near the decomposing tetrahedrite and bismuth sulfosalts. Element distribution maps (Fig. 10) document also limited mobility of bismuth and its limited uptake into the iron oxides. Some of these supergene Bi minerals were identified with Raman spectroscopy as bismutite

Table 3. Representative electron-microprobe analyses of Fe oxides from the image shown in Fig. 8e from the sample L-33. Point numbers are shown in that image. All analyses can be found in supplementary electronic information. - = below detection limit.

Point	10	11	12	13	15	17	19	20
Al_2O_3	0.04	0.09	0.19	0.06	0.07	-	0.06	0.09
As_2O_5	0.91	1.20	1.11	0.68	0.44	0.60	0.65	0.67
SiO_2	0.34	0.59	0.58	0.39	0.33	0.37	0.39	0.43
MgO	-	0.06	0.04	-	-	0.03	0.04	-
SO_3	0.06	0.13	0.11	0.04	-	-	-	0.09
CaO	0.09	0.22	0.28	0.15	0.07	0.11	0.10	0.15
Ag_2O	-	0.05	-	-	-	-	-	0.06
Sb_2O_5	1.25	2.11	1.82	1.31	1.14	1.13	1.42	1.47
HgO	-	-	0.04	0.07	0.04	-	-	0.06
P_2O_5	2.29	5.00	5.20	4.18	2.95	3.08	3.75	3.64
PbO	0.10	-	-	0.05	0.10	0.04	-	-
Bi_2O_3	0.17	0.44	0.38	0.57	0.51	0.53	0.56	0.55
BaO	-	-	-	-	-	-	-	-
MnO_2	-	-	0.39	0.11	0.10	0.10	0.12	0.12
Fe_2O_3	28.52	63.07	65.00	78.42	59.07	62.44	80.55	77.69
CuO	4.05	8.91	8.58	5.73	4.10	3.52	5.52	5.24
ZnO	-	-	-	-	-	-	-	-
CoO	-	-	-	-	-	-	-	-
Total	**37.82**	**81.87**	**83.72**	**91.76**	**68.92**	**71.94**	**93.16**	**90.27**

Table 4. Representative electron-microprobe analyses of Fe oxides, Mn oxides, and pseudomalachite from the image shown in Fig. 8f from the sample L-33. Point numbers are shown in that image. Very low totals of the Mn oxides are caused by the porosity of the fine-grained acicular crystals. All analyses can be found in the supplementary electronic information. - = below detection limit.

Point	29	30	32	36	27	31	34	39
Mineral	Fe-ox	Fe-ox	Fe-ox	Fe-ox	Mn-ox	Mn-ox	Mn-ox	pseudomalachite
Al_2O_3	0.10	0.10	0.20	-	0.04	-	0.05	0.04
As_2O_5	1.05	0.99	1.07	0.81	0.07	-	-	0.91
SiO_2	0.39	0.41	0.38	0.34	0.09	0.07	0.07	-
MgO	0.09	0.06	-	-	0.05	0.03	-	-
SO_3	-	0.07	-	0.05	0.12	0.05	0.06	0.05
CaO	0.18	0.20	0.12	0.15	0.12	0.10	0.05	0.05
Ag_2O	-	-	-	0.08	-	0.04	0.04	-
Sb_2O_5	1.36	1.08	1.04	1.43	0.26	-	0.08	0.06
HgO	0.08	-	-	0.05	-	-	0.06	-
P_2O_5	3.58	3.67	4.23	2.72	0.48	0.07	0.10	23.09
PbO	0.07	0.03	0.03	0.03	0.23	0.08	-	-
Bi_2O_3	0.81	0.77	0.93	0.53	1.32	0.27	0.13	0.07
BaO	-	0.04	-	-	0.59	0.83	0.55	0.15
MnO_2	0.75	0.50	0.44	0.76	13.55	16.61	12.35	
Fe_2O_3	77.38	73.30	75.68	67.41	4.17	1.46	1.53	0.04
CuO	5.97	4.62	4.32	3.36	5.07	6.20	5.20	69.18
ZnO	-	-	-	-	-	-	-	-
CoO	-	-	-	-	1.78	3.26	2.92	-
Total	**91.81**	**85.85**	**88.44**	**77.72**	**27.94**	**29.06**	**23.20**	**93.64**

(Fig. 11) and confirmed previous identification of the mineral (Milovská et al. 2014b).

The iron oxides in the massive aggregates are rich in P_2O_5 (average 2.78 wt.%), SiO_2 (1.67), Al_2O_3 (0.22), and CuO (6.47) (Tables 3 and 4). The high content of P_2O_5 agrees well with the abundance of the supergene phosphates. In the iron oxides, phosphorus is much more abundant than arsenic, with the P_2O_5/As_2O_5 (on a weight basis) being ~10 on average. The concentration of CuO is unusually high, but it is not clear if copper is truly associated with the iron oxides or is found as submicroscopic inclusions (Cu sulfides or native copper) in the mass of these minerals.

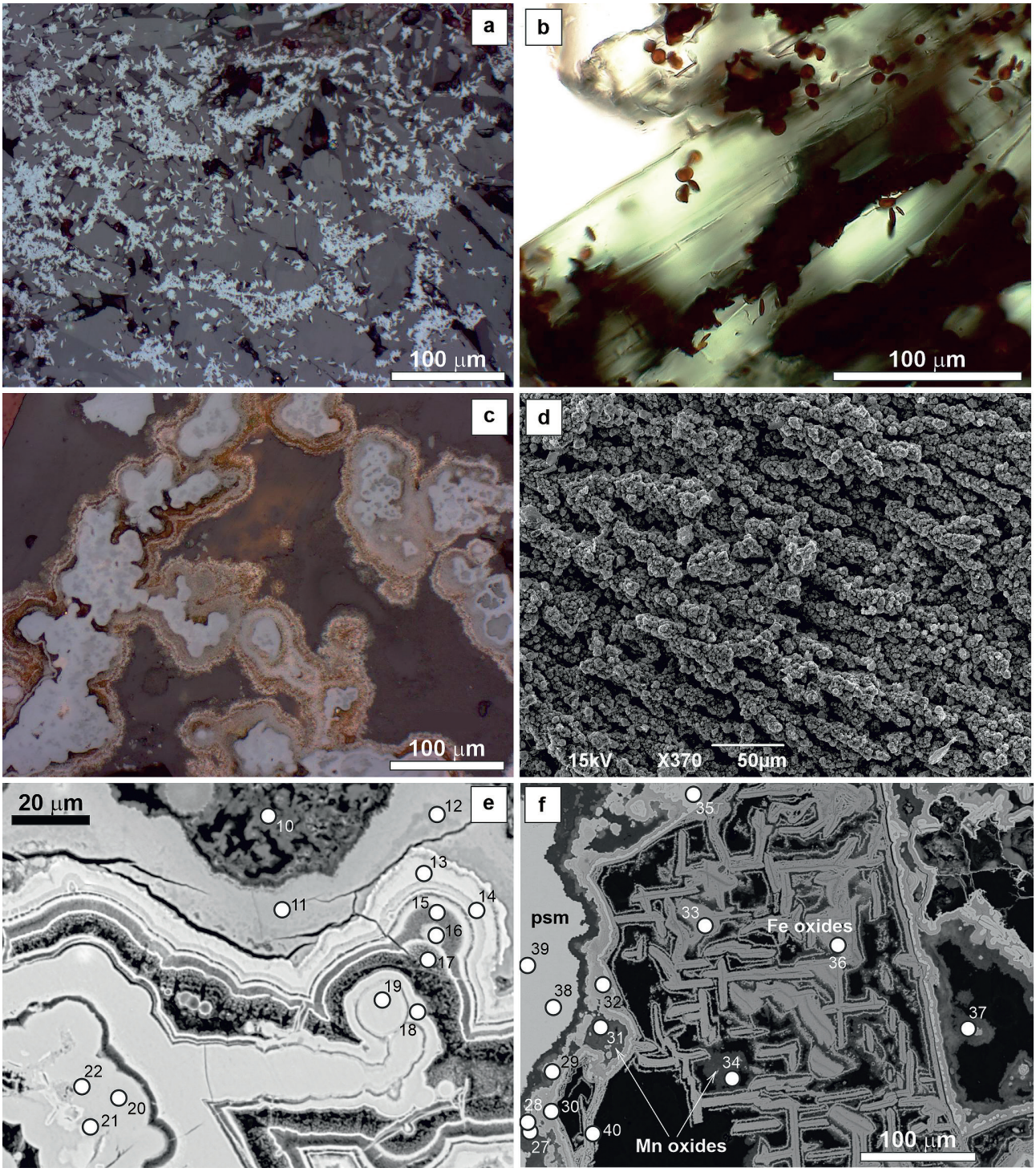

Fig. 8. Iron oxides and associated minerals from Ľubietová. a) Hematite crystals in pseudomalachite (sample L-5, reflected plane-polarized light). b) Thick tabular hematite crystals embedded in pseudomalachite (sample L-5, transmitted plane-polarized light). c) Globular aggregates of Fe oxides, overgrown by a layer of acicular Mn oxides (sample L-33, reflected plane-polarized light). d) Tufts of Fe oxide crystals, morphologically similar to the section shown in c) (sample L-125, secondary electron image). e) Back-scattered electron image of crustiform Fe oxides, both compact and porous (sample L-33). f) Back-scattered electron image of Fe oxides associated with Mn oxides and pseudomalachite (psm) (sample L-33). For e,f): Chemical analyses from these aggregates are listed in Tables 3 and 4 and correspond to the analyses numbers shown in the images.

The ubiquitous coatings of Fe oxides consist mostly of goethite (Fig. 12). Occasionally, hematite was also detected. Because the coatings are only thin films that cover rock fragments, they were not chemically analyzed.

4. CONCLUSIONS

Iron and manganese oxides are an integral part of the oxidation zone at Ľubietová-Podlipa. They are as abundant, if not

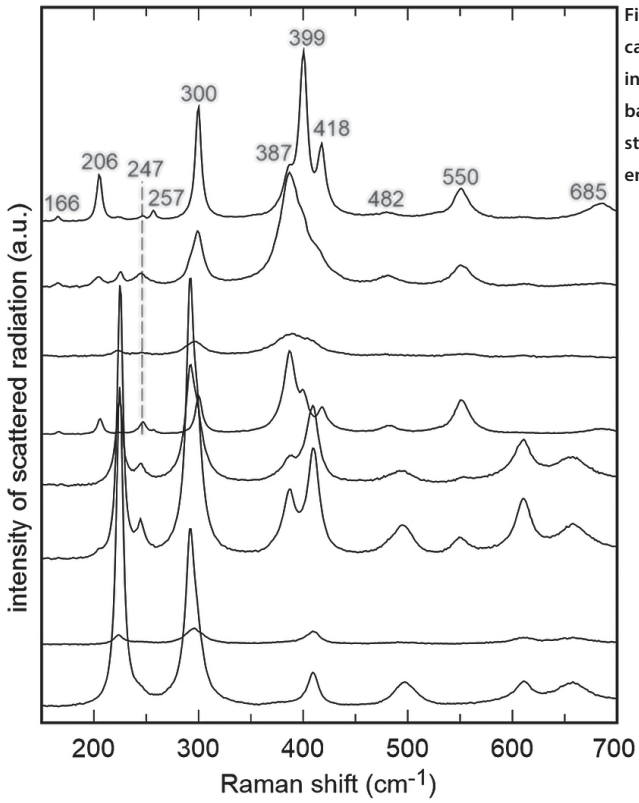

Fig. 9. Raman spectra of massive Fe oxides from Ľubietová. The spectra are vertically offset for clarity. The spectra correspond mostly to goethite, sometimes in a mixture with hematite. No spectra are shown for comparison because the bands visible depend on the orientation and the appearance of the spectra may strongly vary. For more details on the spectral variations of goethite and reference spectra, see Abrashev et al. (2020).

more abundant, than the supergene copper minerals that made this locality famous. The Fe oxides are mixtures of goethite and hematite. The Mn oxides belong to birnessite or asbolane, with a small fraction of tectomanganates (hollandite-like phases).

The temporal relationship between the Fe and Mn oxides and the Cu minerals is variable. It was dictated by the rate of weathering of primary minerals, the rate of Fe/Mn oxidation in the aqueous phase, and the rate of phosphate supply into the oxidation zone. The differences in the chemical composition of the Fe and Mn oxides conform to the observations made elsewhere. They are determined by the tendency of the Fe oxides to preferentially adsorb anions (phosphate, arsenate, silicate) and the tendency of the Mn oxides to adsorb and uptake cations (Co, Ba, K). To a limited extent, Fe oxides also harvest Sb and Bi, but these elements are rare at Podlipa. Still, bulk Bi concentration exceeds that of Sb or As, and such disproportion is unusual for most ore

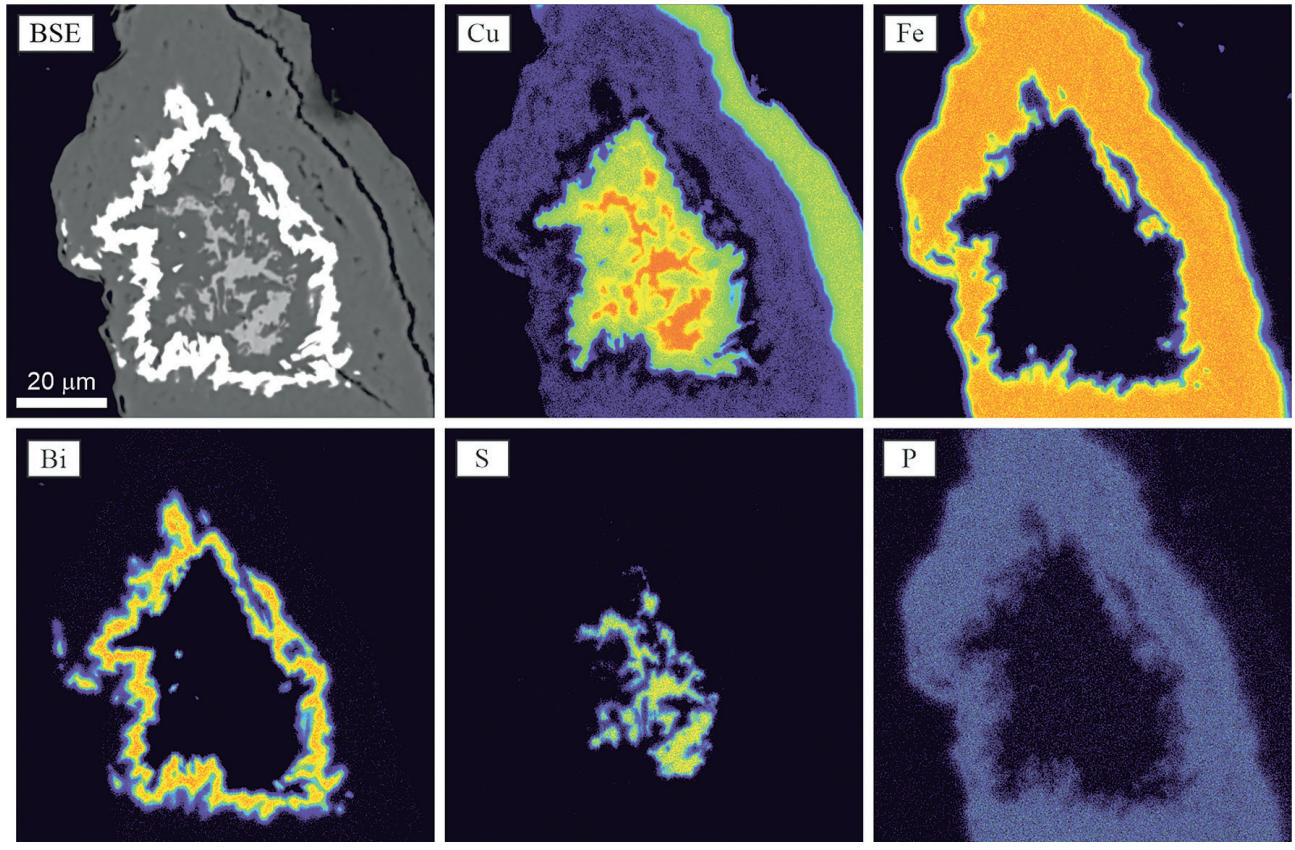

Fig. 10. Element distribution maps, sample L-105. Iron oxides coat partially decomposed grains of sulfides with a supergene Cu sulfide in the middle of the aggregate. The aggregate probably also contained Cu-Bi sulfosalt. Iron oxides are coated with malachite. Note the elevated concentration of P_2O_5 in the iron oxides. Data acquired by an electron microprobe.

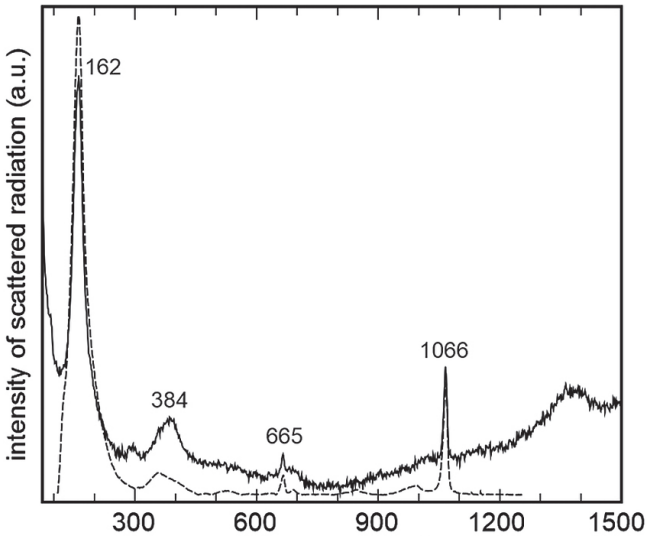

Fig. 11. Raman spectrum of bismutite from Ľubietová (solid curve), compared to the bismutite entry in the RRUFF database (dashed curve) (Lafuente et al. 2015). The values in the figure specify the band position for the sample from Ľubietová.

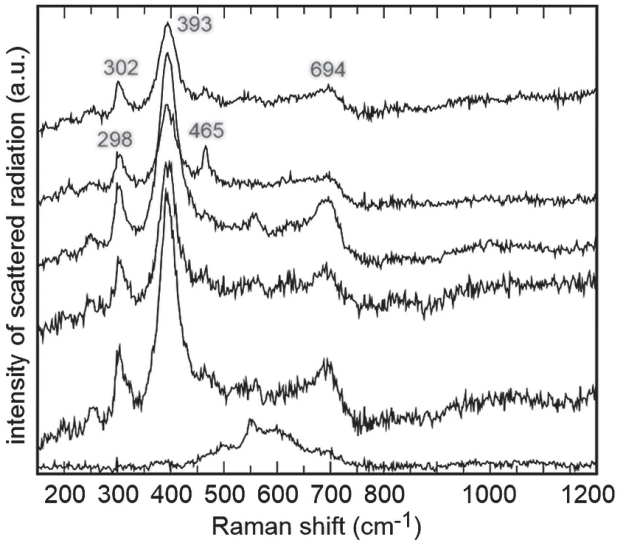

Fig. 12. Raman spectra of the Fe oxide coatings on the host rocks. The bottom spectrum represents a mixture of Fe and Mn oxides. Positions of the most prominent bands were marked with the numerical value of their Raman shift.

bodies. In the case of the locality studied, it can be explained by the minute amount of tetrahedrite, even when compared to the abundance of bismuth sulfosalts.

At Podlipa, phosphate concentration in the Fe oxides is higher than that of arsenate, simply because primary As carriers are scarce. The Fe oxides were able to restrict phosphate availability in the oxidation zone and perhaps also determine whether libethenite (with Cu/P ratio of 2) or pseudomalachite (Cu/P of 2.5) will be formed in a certain volume of the oxidation zone.

Acknowledgements. We appreciate constructive criticism from Zdeněk Losos and Jiří Sejkora and the editor Peter Bačík. Their reviewer comments helped to improve the manuscript. We are thankful to Monika Orvošová and Pavol Herich for underground mapping at Reiner and to Michael Ude for his assistance with the XRF analyses. This study was financially supported by project APVV-22-0041.

References

Abrashev M. V., Ivanov V. G., Stefanov B. S., Todorov N. D., Rosell J. & Skumryev, V., 2020: Raman spectroscopy of alpha-FeOOH (goethite) near antiferromagnetic to paramagnetic phase transition. *Journal of Applied Physics*, 127, 205108.

Breithaupt A., 1823: Vollständige Charakteristik des Mineral-System´s. Arnoldische Buchhandlung, Dresden und Leipzig, 1–358.

Figuschová M., 1977: Secondary copper minerals from Ľubietová. Volume of Abstracts, *Ore-forming Processes in the Western Carpathians*, Bratislava, 135–137. [in Slovak]

Guilbert J. M. & Park C. F., 2007: Geology of Ore Deposits. Waveland Press, 985 p.

González A.G., Pérez-Almeida N., Santana-Casiano J.M., Millero F.J. & González-Dávila M., 2016: Redox interactions of Fe and Cu in seawater. *Marine Chemistry*, 179, 12–22.

Hanesch M., 2009: Raman spectroscopy of iron oxides and (oxy)hydroxides at low laser power and possible applications in environmental magnetic studies. *Geophysical Journal International*, 177, 941–948.

Hyršl J., 1991: Three polymorphs of $Cu_5(PO_4)_2(OH)_4$ from Ľubietová, Czechoslovakia. *Neues Jahrbuch für Mineralogie, Monatshefte*, 6, 281–287.

Koděra M., (ed.) 1990: Topographic Mineralogy of Slovakia, Band 2. Veda, Bratislava, 1590 p. [in Slovak]

Lafuente B., Downs R. T., Yang H. & Stone N., 2015: The power of databases: the RRUFF project. In: *Highlights in Mineralogical Crystallography*, Armbruster T. & Danisi, R.M. De Gruyter, 1–30.

Láznička P., 1965: Cyanotrichite from the copper deposit Ľubietová. *Acta Universitatis Carolinae – Geologica*, 3, 149–155. (in Czech)

Luptáková J., Milovská S., Biroň A., Jeleň S. & Andráš P., 2012: Study of secondary minerals of abandoned Cu deposit Ľubietová-Podlipa (Slovakia). *Acta Mineralogica Petrographica*, Abstract Series, 7, 80.

Luptáková J., Milovská S., Jeleň S., Mikuš T., Milovský R. & Biroň A., 2016: Primary ore Cu mineralization at the Ľubietová-Podlipa locality (Slovakia). *AGEOS*, 8, 175–194.

Majzlan J., Števko M., Chovan M., Luptáková J., Milovská S., Milovský R., Jeleň S., Sýkorová M., Pollok K., Göttlicher J. & Kupka D., 2018: Mineralogy and geochemistry of the copper-dominated neutral mine drainage at the Cu deposit Ľubietová-Podlipa (Slovakia). *Applied Geochemistry*, 92, 59–70.

Majzlan J., *Števko* M., Vďačný M., Milovský R., Milovská S., Jeleň S., Chovan M., Gerdes A. & Herich, P., 2025: Biological and geological contribution to the formation and preservation of copper oxidation zones in central Slovakia. *Mineralogical Magazine*, *in press*.

Manceau A., Llorca S. & Calas, G., 1987: Crystal chemistry of cobalt and nickel in lithiophorite and asbolane from New Caledonia. *Geochimica et Cosmochimica Acta*, 51, 105–113.

Milovská S., Luptáková J., Jeleň S., Biroň A., Lazor P. & Polák Ľ., 2014a: Manganese oxides and oxyhydroxides from Banská Štiavnica, Ľubietová and Selce (central Slovakia). *CEMC 2014*, Book of Abstracts, 94–95.

Milovská S., Luptáková J., Biroň A. & Jeleň S., 2014b: Mineralogy of Ľubietová-Podlipa deposit (the new data). In: Andráš, P., Dirner, V., Turisová, I.,

Vojtková, H. (eds): Old mining pollution legacy of abandoned Cu deposits. Ekomonitor, 166–188. [in Slovak]

Post J. E., 1999: Manganese oxide minerals: Crystal structures and economic and environmental significance. *Proceedings of the National Academy of Sciences USA*, 96, 3447–3454.

Řídkošil T., Šrein V., Fábry J., Hybler J. & Maximov B.A., 1992: Mrázekite, $Bi_2Cu_3(OH)_2O_2(PO_4)_2{\cdot}2H_2O$, a new mineral species and its crystal structure. *Canadian Mineralogist*, 30, 215–224.

Števko M., Sejkora J. & Malíková R., 2016: New data on supergene minerals from the ore field Rainer, Ľubietová-Podlipa deposit (Slovak Republic). *Bulletin Mineralogie a Petrologie*, 24, 1–12. [in Slovak]

Števko M., Sejkora J. & Dolníček Z., 2021: Olivenite and cornwallite from the Podlipa copper deposit near Ľubietová, Slovakia. *Bulletin Mineralogie a Petrologie*, 29, 189–196.

Števko M., Sejkora J. & Súľovec Š., 2017: Contribution to the chemical composition of libethenite from the type locality: Podlipa copper deposit, Ľubietová (Slovak Republic). *Bulletin Mineralogie a Petrologie*, 25, 252–259.